

# Sensitizing Curium Luminescence through an Antenna Protein To Investigate Biological Actinide Transport Mechanisms

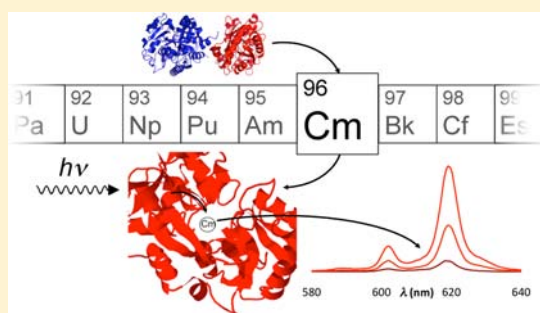
Manuel Sturzbecher-Hoehne,<sup>†</sup> Christophe Goujon,<sup>†</sup> Gauthier J.-P. Deblonde,<sup>†</sup> Anne B. Mason,<sup>‡</sup> and Rebecca J. Abergel<sup>\*†</sup>

<sup>†</sup>Chemical Sciences Division, The Glenn T. Seaborg Center, Lawrence Berkeley National Laboratory, Berkeley, California 94720, United States

<sup>‡</sup>Department of Biochemistry, University of Vermont College of Medicine, Burlington, Vermont 05405-0068, United States

**S** Supporting Information

**ABSTRACT:** Worldwide stocks of actinides and lanthanide fission products produced through conventional nuclear spent fuel are increasing continuously, resulting in a growing risk of environmental and human exposure to these toxic radioactive metal ions. Understanding the biomolecular pathways involved in mammalian uptake, transport and storage of these f-elements is crucial to the development of new decontamination strategies and could also be beneficial to the design of new containment and separation processes. To start unraveling these pathways, our approach takes advantage of the unique spectroscopic properties of trivalent curium. We clearly show that the human iron transporter transferrin acts as an antenna that sensitizes curium luminescence through intramolecular energy transfer. This behavior has been used to describe the coordination of curium within the two binding sites of the protein and to investigate the recognition of curium–transferrin complexes by the cognate transferrin receptor. In addition to providing the first protein–curium spectroscopic characterization, these studies prove that transferrin receptor-mediated endocytosis is a viable mechanism of intracellular entry for trivalent actinides such as curium and provide a new tool utilizing the specific luminescence of curium for the determination of other biological actinide transport mechanisms.



## INTRODUCTION

In the event of an accidental release of radiological/nuclear material into the environment, radionuclides such as actinides (An) and lanthanide (Ln) fission products are a severe health risk as contaminants, due to both radiological and chemical toxicities.<sup>1</sup> While increasing amounts of the trivalent minor An(III) curium (Cm) and americium (Am) are produced through conventional nuclear spent fuel<sup>2</sup> and efforts to optimize separation processes between Cm, Am, and Ln(III) have recently intensified,<sup>3</sup> the biochemical mechanisms associated with uptake, transport and storage of these toxic metal ions remain largely unexplored. Independent of the contamination pathway, An(III) are known to rapidly transit in the bloodstream and predominantly deposit in the liver and skeleton, with very slow subsequent elimination from the organism.<sup>1,4,5</sup> Understanding the thermodynamics and kinetics of complexation of these metals by endogenous ligands is therefore extremely important not only to determine their biological speciation, but also to transpose the high affinity and selectivity of the coordination sites in these natural species into new ligand systems for the development of potential decontamination and separation strategies.<sup>3,6</sup>

In the past, very few studies have investigated the distribution of An(III) in blood and natural body fluids.<sup>7</sup> In addition to forming small inorganic species as well as ultrafilterable citrate

complexes, Cm<sup>3+</sup> and Am<sup>3+</sup> are quantitatively bound to some major plasma proteins including the iron-transport protein transferrin (Tf).<sup>5,8–10</sup> Human serum Tf is a ~80 kDa glycoprotein that binds Fe<sup>3+</sup> reversibly and controls the concentration of extracellular iron in the bloodstream; it is comprised of a single polypeptide chain with two homologous lobes, the N- and C-lobes.<sup>11</sup> Each lobe contains a well characterized binding-cleft that can tightly coordinate a single ferric ion through two tyrosine residues, one monodentate aspartate, one histidine and a bidentate synergistic carbonate anion, in a distorted octahedral geometry (Figure 1).<sup>12</sup> Physiologically, one molecule of diferric Tf (Fe<sub>2</sub>Tf) binds tightly to each monomer of the homodimeric Tf receptor (TfR) located on the extracellular surface of actively dividing cells, forming a complex that can undergo endocytosis and subsequently releases iron at the putative endosomal pH, while cycling the now iron-free Tf (apo-Tf) back to the plasma membrane (Figure 1).<sup>13</sup> This mechanism is highly specific and selective: while apo-Tf is poorly recognized by the receptor, the respective TfR-affinities of both monoferric species Fe<sub>C</sub>Tf and Fe<sub>N</sub>Tf (where a single Fe<sup>3+</sup> is bound to the C-lobe or the N-lobe, respectively) are approximately 40-fold weaker than that

Received: November 6, 2012

Published: January 30, 2013

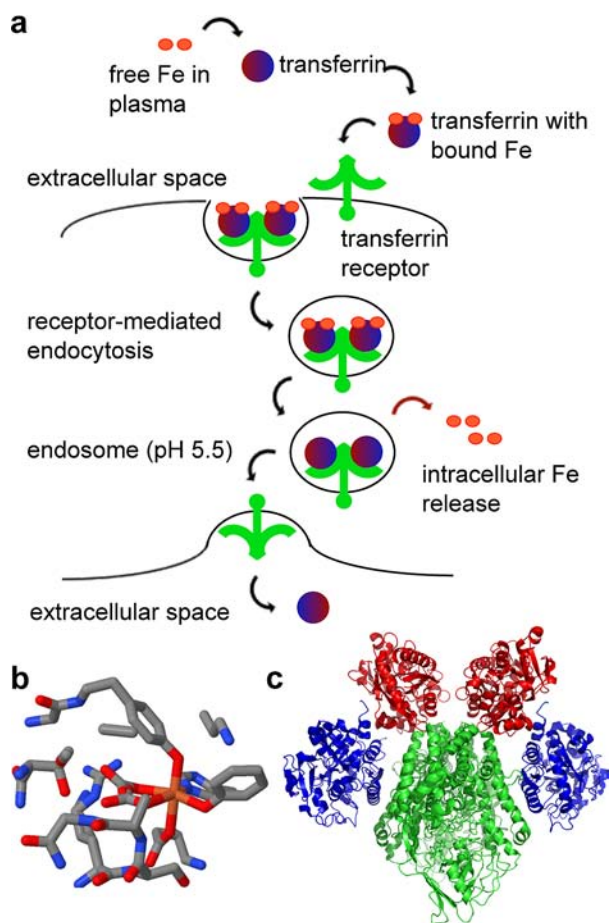


**Figure 1.** TfR-mediated intracellular iron uptake. (a) Once bound to two  $\text{Fe}^{3+}$  ions, the complex  $\text{Fe}_2\text{Tf}$  is recognized by the TfR membrane receptor and internalized via endocytosis; metal release occurs at endosomal pH. This is the proposed pathway for intracellular uptake of exogenous metals such as  $\text{Cm}^{3+}$ . (b) Metal binding site of the Tf N-lobe, with Tyr 188, Tyr 95, His 249, Asp 63 and a synergistic carbonate anion participating in the coordination of  $\text{Fe}^{3+}$ .<sup>14</sup> (c) Structure of the  $(\text{Tf})_2\text{-TfR}$  complex, with TfR in green, Tf N-lobes in red) and Tf C-lobes in blue, adapted from previously reported X-ray data.<sup>15</sup>

of  $\text{Fe}_2\text{Tf}$ , and the kinetic rates of intracellular Fe release from each Tf lobe are different.<sup>16</sup> However, this tightly controlled pathway may not be completely effective in discriminating between  $\text{Fe}^{3+}$  and other metal ions and is still considered a possible mechanism of intracellular entry for some exogenous toxic metals.

As previously reported, ytterbium ( $\text{Yb}^{3+}$ ) may rapidly accumulate inside cells through TfR-mediated endocytosis of  $\text{Yb}_2\text{Tf}$ .<sup>17</sup> In contrast, a variety of spectroscopic studies have proposed that the conformation of the Tf complex formed with the dioxo cation uranyl ( $\text{UO}_2^{2+}$ ) prevents binding to TfR.<sup>18,19</sup> Finally, a subtler uptake pathway has recently been described for plutonium ( $\text{Pu}^{4+}$ ), in which neither  $\text{Pu}_2\text{Tf}$  nor  $\text{Fe}_C\text{Pu}_N\text{Tf}$  can undergo endocytosis and only the mixed  $\text{Pu}_C\text{Fe}_N\text{Tf}$  complex seems to specifically bind TfR.<sup>20</sup> These results imply that the TfR-mediated uptake of metal-bound Tf ( $\text{M}_2\text{Tf}$ ) is a highly selective system based on the oxidation state, charge, and size of the metals, as well as on the conformation of the resulting  $\text{M}_2\text{Tf}$ . Unfortunately, no comparable data is available for An(III) because of their high specific radioactivities with resulting experimental constraints.

$\text{Cm(III)}$  exhibits unique luminescence properties that can provide detailed information on the metal coordination and allow experimental work at very low concentrations and specific activities.<sup>21</sup> Taking advantage of this peculiarity, the present study describes the first example of  $\text{Cm(III)}$  emission sensitization by a macromolecular entity, namely the protein Tf, through an intramolecular energy transfer process known as the antenna effect.<sup>22,23</sup> The distinct luminescent features of the  $\text{Cm}_2\text{Tf}$  and  $\text{Fe}_C\text{Cm}_N\text{Tf}$  complexes were established and used to characterize the coordination of  $\text{Cm(III)}$  within the protein metal-binding sites, as well as the recognition of these complexes by TfR. The thermodynamic constants associated with the sequential complexation of  $\text{Cm(III)}$  by Tf and the binding of  $\text{Cm}_2\text{Tf}$ ,  $\text{Fe}_C\text{Cm}_N\text{Tf}$ , and  $\text{Cm}_C\text{Fe}_N\text{Tf}$  by TfR provide some mechanistic insights into the different distribution profiles and organ uptake rates observed with various actinides. These results also raise the question of whether discriminating biological systems such as the Tf/TfR metal-uptake pathway could be revisited and used to develop efficient *in vitro* separation processes.

## EXPERIMENTAL SECTION

**General.** All chemicals were obtained at the highest available grade from commercial suppliers and were used as received. All aqueous solutions were prepared using deionized water purified with a Millipore Milli-Q reverse osmosis cartridge system. All spectroscopic measurements were performed at 25 °C. Caution: curium radioisotopes must be handled in facilities designed for the safe manipulation of transuranic elements. Before performing studies with  $\text{Cm}^{3+}$ , all experimental protocols were established using  $\text{Eu}^{3+}$  (corresponding data and results are shown as Supporting Information).

**Preparation of Protein Solutions.** Human apo-Tf (98% iron free, Sigma) was used to prepare stock solutions of apo-Tf, diferric  $\text{Fe}_2\text{Tf}$ , and monoferric  $\text{Fe}_C\text{Tf}$  and  $\text{Fe}_N\text{Tf}$  in Tris buffer (50 mM Tris, pH 8.6, 150 mM NaCl, 5 mM  $\text{NaHCO}_3$ ) for metal-binding studies or in 100 mM  $\text{NH}_4\text{CO}_3$  (pH 7.4) for receptor-binding studies, following previously published methods.<sup>24,25</sup> The Eu- and Cm-loaded protein complexes were freshly prepared by addition of adequate equivalents of  $\text{EuCl}_3$  (standardized 0.1 M HCl stock solution) or  $\text{CmCl}_3$  (standardized 1 M HCl stock solution; 96%  $^{248}\text{Cm}$ , 4%  $^{246}\text{Cm}$  isotopic distribution) to apo-Tf,  $\text{Fe}_C\text{Tf}$ , or  $\text{Fe}_N\text{Tf}$ . All transferrin solutions were purified on Sephadex G-25 columns (PD-10 column, GE Healthcare) and were stored at 4 °C until use. The respective protein concentrations and percentage of metal saturation were determined by UV-visible spectroscopy.<sup>25</sup> Recombinant His-tagged sTfR was produced and purified from a BHK cell expression system, as previously described.<sup>26</sup> Solutions of sTfR were stored in 100 mM  $\text{NH}_4\text{HCO}_3$  at pH 7.4 at 4 °C until use.

**Photophysical Characterization.** UV-visible absorption spectra were recorded either on a Varian Cary 5000 or Varian Cary 6000 double beam absorption spectrometer, using quartz cells of 1.00 cm path length. Emission spectra and lifetimes were acquired on a HORIBA Jobin Yvon IBH FluoroLog-3 spectrofluorimeter, as described elsewhere.<sup>27</sup> Luminescence spectra using the absorption maximum of the protein ( $\lambda_{\text{exc}} = 280$  nm) for excitation were acquired with 3–1 nm slits, while slits were adjusted to 14–7 nm for direct excitation of  $\text{Cm}^{3+}$  ( $\lambda_{\text{exc}} = 397$  nm). Goodness of fit was assessed by minimizing the reduced chi squared function,  $\chi^2$ , and a visual inspection of the weighted residuals. Each trace contained 10 000 points, and the estimated error on the reported lifetime values is  $\pm 10\%$ . Quantum yields were determined by the optical dilute method, using an excitation wavelength of 275 nm and tyrosine as a reference standard ( $\Phi_r = 0.14$ ).<sup>28,29</sup> Procedures for the data treatment of quantum yields and kinetic parameters have been detailed previously.<sup>30</sup>

**Solution Thermodynamics of Metal-Tf Solutions.** A Metrohm Micro Combi glass electrode (response to  $[\text{H}^+]$  calibrated daily) was

used to measure the pH of the experimental solutions. Sample solutions were assembled from stock solutions of apo-Tf (resulting concentration of  $\sim 10 \mu\text{M}$ ) and the supporting electrolyte solution (50 mM Tris, pH 8.6, 150 mM NaCl, 5 mM  $\text{NaHCO}_3$ ) and were incrementally perturbed by the addition of 1 to 10  $\mu\text{L}$  aliquots of metal titrant (including  $\text{EuCl}_3$ ,  $\text{CmCl}_3$ , and solutions of  $[\text{Eu}(\text{NTA})]$ ,  $[\text{Eu}(\text{NTA})_2]^{3-}$ ,  $[\text{Eu}(\text{EDDA})]^+$ , or  $[\text{Cm}(\text{NTA})]$  prepared from the acidic stocks according to described procedures,<sup>25</sup> followed by a time delay for equilibration (10 to 60 min). Each data point consisted of a UV-visible spectrum ( $\lambda = 220\text{--}350 \text{ nm}$ ) for Eu- and Cm-containing samples, and emission spectra ( $\lambda_{\text{exc}1} = 280 \text{ nm}$ ,  $\lambda_{\text{exc}2} = 397 \text{ nm}$ ,  $\lambda_{\text{em}} = 420\text{--}750 \text{ nm}$ ), excitation spectra ( $\lambda_{\text{em}1} = 602 \text{ nm}$ ,  $\lambda_{\text{em}2} = 619 \text{ nm}$ ,  $\lambda_{\text{exc}} = 240\text{--}320 \text{ nm}$ ), and lifetime measurements (kinetic traces observed at 602 and 619 nm for excitation at 280 and 397 nm, respectively) for Cm-containing samples. All spectra were corrected for dilution occurring during titrations. Absorptivity and emission data sets were imported into the refinement program HypSpec<sup>31–34</sup> and analyzed by nonlinear least-squares refinement.

**HPLC sTfR Binding Assay.** All High Pressure Liquid Chromatography runs were performed on an Agilent 1200 Series LC module, by injection of 9  $\mu\text{L}$  through a gel filtration ZORBAX GF-250 ( $4.6 \times 250 \text{ mm}$ ,  $4 \mu\text{m}$ ) column. An isocratic method with 100 mM  $\text{NH}_4\text{HCO}_3$ , pH 7.4, over 40 min at  $0.1 \text{ mL min}^{-1}$  was applied to elute the proteins and protein complexes. Detection of the different species was achieved by UV-visible absorption (multi wavelength detector tuned at 210, 240, 278, 320, and 440 nm) and fluorescence emission ( $\lambda_{\text{exc}} = 278 \text{ nm}$ ,  $\lambda_{\text{em}1} = 380 \text{ nm}$ ,  $\lambda_{\text{em}2} = 619 \text{ nm}$ ). Solutions of Tf-sTfR complexes were prepared by mixing sTfR with aliquots of apo-Tf or metal-loaded Tf solutions in 100 mM  $\text{NH}_4\text{HCO}_3$ , with minimum equilibration times of 40 min before injection. Chromatograms were first deconvoluted with a Gaussian function based on maximum peak values for each observed species and with a Lorentzian function to include peak shape in the fits. Equilibrium dissociation constants ( $K_{d1}$  and  $K_{d2}$ ) were then determined by nonlinear regression analysis of peak areas vs protein concentration using a two-site binding model as implemented in the refinement program Dynafit.<sup>35</sup>

## RESULTS

### Spectroscopic Characterization of Cm-Tf Complexes.

The electronic absorption spectrum of apo-Tf, with an absorption maximum at  $\lambda_{\text{max}} = 280 \text{ nm}$  varies only slightly upon addition of  $\text{CmCl}_3$ . These changes were followed for the addition of up to 2.6 equiv of  $\text{CmCl}_3$  (1 and 2 equiv corresponding to the formation of  $\text{Cm}_1\text{Tf}$  and  $\text{Cm}_2\text{Tf}$ , respectively) through difference ultraviolet spectra (Figure 2a). The growth of bands at 247 and 295 nm is characteristic of metal ion binding to the tyrosine residues at the two Tf binding sites.<sup>25</sup> Corresponding luminescence spectra were acquired using the absorption maximum of the protein ( $\lambda_{\text{exc}} = 280 \text{ nm}$ ) (Figure 2b). A broad emission band centered at  $\lambda_{\text{em}} = 330 \text{ nm}$  is attributed to the fluorescence of the aromatic amino acids of the protein (data not shown),<sup>29</sup> while a characteristic  $\text{Cm}^{3+}$  emission corresponding to the intense  ${}^6\text{D}_{7/2} \rightarrow {}^8\text{S}_{7/2}$  hypersensitive transition results in bright orange luminescence, with sharp peaks at  $\lambda_{\text{em}} = 619, 602, \text{ and } 588 \text{ nm}$  ( $\nu_{\text{em}} = 16155, 16611, \text{ and } 17007 \text{ cm}^{-1}$ , respectively).<sup>36</sup> This structured 3-peak emission is attributed to ligand field splitting of the emitting state  $J = 7/2$ , as the spherical symmetry of the  $\text{Cm}^{3+}$  half-filled  $5f^7$  configuration should only result in a small splitting due to inner sphere coordinating ligands.<sup>36,37</sup> The most intense emission band at 619 nm (85%) is assigned as originating from the lowest Stark level of the  $J = 7/2$  excited state, while the higher energy splittings at 602 nm (12%) and 588 nm (3%) are remaining Stark components. No luminescence was observed upon direct excitation of the  $\text{Cm}^{3+}$  ions at  $\lambda_{\text{exc}} = 397 \text{ nm}$  under similar measurement conditions. However, an

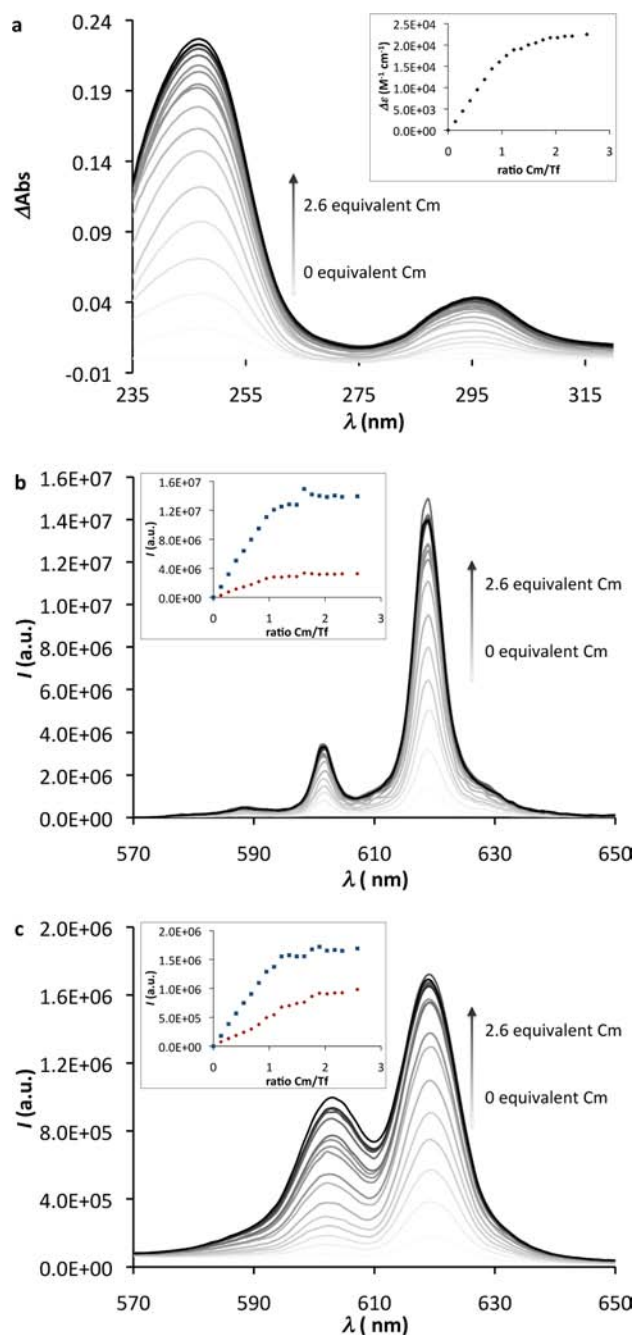


**Figure 2.** Spectroscopic titrations showing the sequential binding of two  $\text{Cm}^{3+}$  ions by Tf (50 mM Tris, pH 8.6, 150 mM NaCl, 5 mM  $\text{NaHCO}_3$ ,  $25 \text{ }^\circ\text{C}$ ); apo-Tf solutions (1.5 mL,  $10.3 \mu\text{M}$ ) were incrementally perturbed by addition of  $\text{CmCl}_3$  (1.41 mM,  $10 \mu\text{L}$  aliquots). (a) Changes in absorbance spectra, with continuous growth of the broad bands centered at 247 and 295 nm; the inset shows a steady increase of the difference in extinction coefficient as a function of the concentration ratio Cm/Tf. (b) Changes in emission spectra after excitation of the protein at  $\lambda_{\text{exc}} = 280 \text{ nm}$  (slits 3–1 nm); the inset shows intensity changes at both emission peak maxima of 602 nm (red diamond) and 619 nm (blue square) upon  $\text{Cm}^{3+}$  addition. (c) Changes in emission spectra after direct excitation of  $\text{Cm}^{3+}$  at  $\lambda_{\text{exc}} = 397 \text{ nm}$  (slits 14–7 nm); the inset shows intensity changes at both emission peak maxima of 602 nm (red diamond) and 619 nm (blue square) upon  $\text{Cm}^{3+}$  addition.

increased excitation intensity allowed the detection of much broader  $\text{Cm}^{3+}$  emission peaks at  $\lambda_{\text{em}} = 619$  and  $602 \text{ nm}$  (Figure

2c). Such emission profiles are indicative of efficient sensitization of the  $\text{Cm}^{3+}$  luminescence by the complexed protein. Furthermore, excitation spectra monitoring emission at 619 and 602 nm displayed two growing transitions centered at 247 and 287 nm upon addition of  $\text{CmCl}_3$  to apo-Tf (Supporting Information), consistent with energy transfer from tyrosine residues coordinated to the metal ions,<sup>38</sup> in  $\text{Cm}_\text{C}$ Tf and  $\text{Cm}_2$ Tf, resulting in the excitation of  $\text{Cm}^{3+}$  luminescence. This energy transfer is also evidenced by the decrease of the protein luminescence quantum yield ( $\lambda_{\text{exc}} = 280$  nm,  $\lambda_{\text{em}} = 330$  nm) upon Cm binding, from 7.1% for apo-Tf to 6.8% and 6.6% for  $\text{Cm}_\text{C}$ Tf and  $\text{Cm}_2$ Tf, respectively (Table 1).

**Table 1. Photophysical, Thermodynamic Properties, and TfR Affinities of  $\text{Cm}^{3+}$  Complexes of Tf<sup>a</sup>**

Photophysical Parameters						
	$\lambda_{\text{exc}}$	$\epsilon_{\text{exc}}^b$	$\tau\{\text{H}_2\text{O}\}^b$	$\tau\{\text{D}_2\text{O}\}^b$	$\Phi\{\text{H}_2\text{O}\}$	$q$
$\text{Cm}_\text{C}$ Tf			220(22)	476(48)	0.011(1)	2.1(3)
	280,	94200(900)	220(22)			2.1(3)
$\text{Cm}_2$ Tf					0.012(1)	
			206(21) <sup>c</sup>			2.3(3) <sup>c</sup>
Thermodynamic Parameters						
			$\log K_1$	$\log K_2$		$\log \beta$
$\text{Cm}_\text{C}$ Tf	$\text{Cm}_2$ Tf		8.8(3)	7.0(1)		15.8(2)
Binding Affinities toward sTfR						
species			$K_{d1}$ (nM)			$K_{d2}$ (nM)
$\text{Fe}_2$ Tf			5(1)			20(5)
$\text{Cm}_2$ Tf			74(26)			153(77)
$(\text{Fe}_\text{C}\text{Cm}_\text{N})$ Tf			15(24)			42(9)
$(\text{Cm}_\text{C}\text{Fe}_\text{N})$ Tf			3(3)			28(11)

<sup>a</sup>The figures in parentheses give the uncertainties determined from the standard deviation between at least two independent experiments.

<sup>b</sup> $\lambda_{\text{exc}}$  in nm,  $\epsilon_{\text{exc}}$  in  $\text{M}^{-1} \text{cm}^{-1}$ ,  $\tau$  in  $\mu\text{s}$ . <sup>c</sup>Lifetime for the N-terminal site determined using  $\text{Fe}_\text{C}\text{Cm}_\text{N}$ Tf.

In addition, the similar Cm luminescence quantum yields ( $\lambda_{\text{exc}} = 280$  nm,  $\lambda_{\text{em}} = 619$  nm) of  $\text{Cm}_\text{C}$ Tf ( $\Phi = 1.1\%$ ) and  $\text{Cm}_2$ Tf ( $\Phi = 1.2\%$ ) indicate that the C-terminal binding site of the protein has higher sensitization efficiency than the N-terminal binding site. Time-resolved analysis of  $\text{Cm}_\text{C}$ Tf, measured at 619 nm in  $\text{H}_2\text{O}$  and  $\text{D}_2\text{O}$ , revealed monoexponential decays with lifetimes of ca. 220 and 476  $\mu\text{s}$ , respectively (Figure 3). A similar decay time in  $\text{H}_2\text{O}$  was measured for  $\text{Cm}_2$ Tf, most likely due to the predominant brightness of the C-terminal binding site. The monoexponential decay associated to the Cm-bound N-terminal site of the protein was observed by blocking the C-terminal site with a ferric ion in  $\text{Fe}_\text{C}\text{Cm}_\text{N}$ Tf, with a corresponding decay time of ca. 206  $\mu\text{s}$  in  $\text{H}_2\text{O}$  (data not shown). Applying a method derived by Kimura et al.,<sup>39</sup> the numbers of inner sphere water molecules were determined as  $q_\text{C} = 2.1$  and  $q_\text{N} = 2.3$ , essentially two, in each binding site (Supporting Information).

#### Solution Thermodynamics of Cm Complexation by Tf.

The sequential binding of metal ions to Tf involves the displacement of protons from the protein and the concomitant binding of a synergistic bicarbonate anion in each binding site.<sup>40</sup> On the basis of kinetic studies that predict formation of the binary bicarbonate-Tf intermediates before metal binding and following previously described analytical methods for the determination of lanthanide-Tf binding constants,<sup>40</sup> two stepwise formation constants ( $K_\text{C}$  and  $K_\text{N}$  for the respective

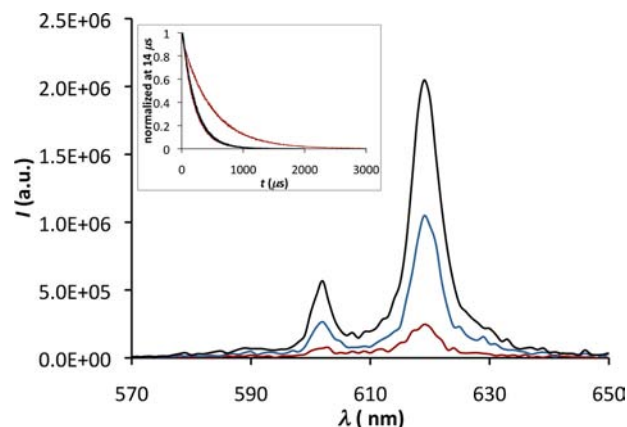


**Figure 3.** Fluorescence spectra of 0.95  $\mu\text{M}$  solutions of  $\text{Cm}_2$ Tf (red),  $(\text{Cm}_2\text{Tf})$ -sTfR (blue), and  $(\text{Cm}_2\text{Tf})_2$ -sTfR (black) in 100 mM  $\text{NH}_4\text{HCO}_3$ , pH 7.4, 25  $^\circ\text{C}$ . The inset shows lifetime measurements at 619 nm upon excitation at 280 nm for all three species in  $\text{H}_2\text{O}$  and for  $\text{Cm}_2$ Tf (dotted red) in  $\text{D}_2\text{O}$ .

binding to the C- and N-lobe) were determined for the complexation of Cm by Tf through four types of spectroscopic titrations in buffered aqueous solutions (pH 8.6 and pH 7.4,  $[\text{NaHCO}_3] \geq 5$  mM). Changes in the UV–visible spectra as well as in the emission spectra (through indirect and direct excitation of  $\text{Cm}^{3+}$  at 280 and 397 nm) were followed upon incremental additions of up to 2.6 equiv of  $\text{CmCl}_3$  to apo-Tf, showing continuous increase in absorption of the broad bands centered at 247 and 295 nm, as well as continuous increase in emission at 619 nm, until a Tf/Cm ratio of 1:2 is reached (Figure 2). Similarly, these spectroscopic features were followed in a reverse titration model, upon incremental additions of up to 4.4 equiv of the competing chelating agent nitrilotriacetic acid (NTA) to  $\text{Cm}_2$ Tf (Figure 4). In this case, absorbance centered at 247 nm decreased with the release of  $\text{Cm}^{3+}$  from Tf and the stepwise formation of the  $[\text{Cm}(\text{NTA})]$  and  $[\text{Cm}(\text{NTA})_2]^{3-}$  complexes. A corresponding decrease in emission intensity was observed after protein excitation at 280 nm, while direct excitation of the  $\text{Cm}^{3+}$  ions at 397 nm allowed for the simultaneous monitoring of the NTA complex formation, with growing emission at 604 nm, diminishing emission at 619 nm and an isosbestic point at 613 nm. Lifetime measurements confirmed the presence of the two distinct  $[\text{Cm}(\text{NTA})]$  and  $[\text{Cm}(\text{NTA})_2]^{3-}$  species.<sup>41</sup> Both  $K_\text{C}$  and  $K_\text{N}$  could be directly calculated from those direct  $\text{CmCl}_3$  and reverse NTA competition titrations. However, the association constants for each binding site of the protein were also determined independently by spectrofluorimetric titrations of (i) apo-Tf with  $[\text{Cm}(\text{NTA})]$  (for  $K_\text{C}$ ) and (ii)  $\text{Fe}_\text{C}$ Tf with  $\text{CmCl}_3$  (for  $K_\text{N}$ ).

Emission spectra and time-resolved analyses were characteristic of the disappearance of the  $[\text{Cm}(\text{NTA})]$  complex and the simultaneous formation of  $\text{Cm}_\text{C}$ Tf in the first case, and of the formation of  $\text{Fe}_\text{C}\text{Cm}_\text{N}$ Tf in the latter case. Least-square refinements, including NTA protonation and Cm-complex formation constants as well as Cm hydrolysis products,<sup>42</sup> were used to analyze the difference ultraviolet spectra and emission spectra for those four direct or competition titrations, providing the two sequential association constants  $\log K_\text{C} = 8.8 \pm 0.3$  and  $\log K_\text{N} = 7.0 \pm 0.1$ , along with an overall formation constant  $\log \beta = 15.8 \pm 0.4$  for  $\text{Cm}_2$ Tf.

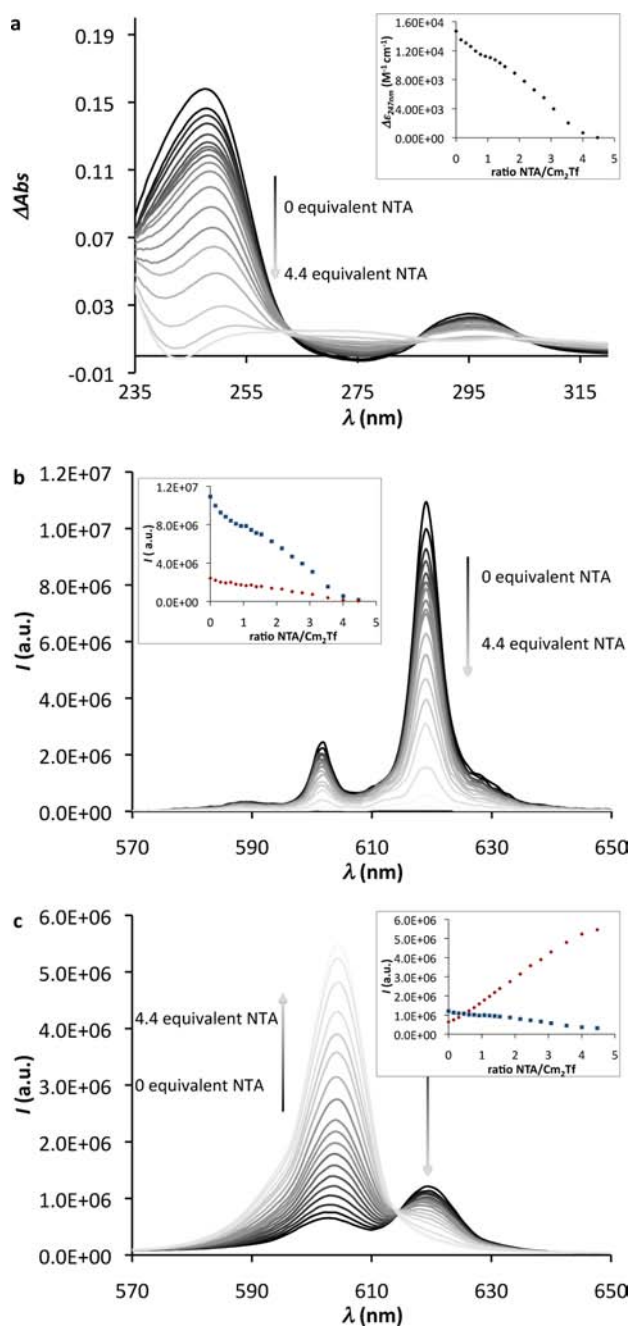


**Figure 4.** Spectroscopic competition titrations of  $\text{Cm}_2\text{Tf}$  against NTA (50 mM Tris, pH 8.6, 25 °C);  $\text{Cm}_2\text{Tf}$  solutions (1.5 mL, 10.4  $\mu\text{M}$ ) were incrementally perturbed by the addition of NTA (0.8 mM, 10  $\mu\text{L}$  aliquots). (a) Changes in absorbance spectra, with continuous decrease of the broad bands centered at 247 and 295 nm; the inset shows a decrease of the difference in extinction coefficient as a function of the concentration ratio NTA/ $\text{Cm}_2\text{Tf}$ . (b) Decrease of emission intensity after excitation of the protein at  $\lambda_{\text{exc}} = 280$  nm (slits 3–1 nm), leading to signal disappearance after 4 equiv of NTA; the inset shows intensity changes at both emission peak maxima of 602 nm (red diamond) and 619 nm (blue square) upon NTA addition. (c) Changes in emission spectra after direct excitation of  $\text{Cm}^{3+}$  at  $\lambda_{\text{exc}} = 397$  nm (slits 14–7 nm); the inset shows intensity changes at both emission peak maxima of 602 nm (red diamond) and 619 nm (blue square) upon  $\text{Cm}^{3+}$  addition.

**Receptor Recognition of  $\text{Cm-Tf}$  Complexes.** The specific luminescence features of  $\text{Cm}_2\text{Tf}$  were utilized to

characterize its recognition by the soluble recombinant sTfR receptor. Emission spectra were recorded for the 1:1 and 2:1 complexes  $(\text{Cm}_2\text{Tf})_2:\text{sTfR}$  and  $(\text{Cm}_2\text{Tf})_2:\text{sTfR}$  prepared *in situ* ( $\lambda_{\text{exc}} = 280$  nm), showing a strong intensity enhancement of the split  $\text{Cm}^{3+}$  emission (at 619, 602, and 588 nm) upon receptor binding (Figure 3). However, the decay time of both species in  $\text{H}_2\text{O}$  remained identical to that of  $\text{Cm}_2\text{Tf}$  at 220  $\mu\text{s}$ , indicating that the  $\text{Cm}^{3+}$  coordination sphere in the Tf binding lobes is not altered upon complexation of the Tf protein by its receptor. A hydrophilic gel-filtration high-performance liquid chromatography (HPLC) assay was designed to separate metal-bound  $\text{M}_2\text{Tf}$  from sTfR,  $(\text{M}_2\text{Tf})_2:\text{sTfR}$ , and  $(\text{M}_2\text{Tf})_2:\text{sTfR}$ , based on their respective sizes and spectroscopic features. Efficient separation of the different protein complexes occurred over 5 min under the chosen experimental conditions and was confirmed using UV–vis spectroscopic detection for  $\text{Fe}_2\text{Tf}$ , while both UV–vis and fluorescence spectroscopies were used to detect  $\text{Cm}_2\text{Tf}$ ,  $\text{Fe}_\text{C}\text{Cm}_\text{N}\text{Tf}$ ,  $\text{Cm}_\text{C}\text{Fe}_\text{N}\text{Tf}$ , and associated receptor complexes (Figure 5). This assay was used to evaluate

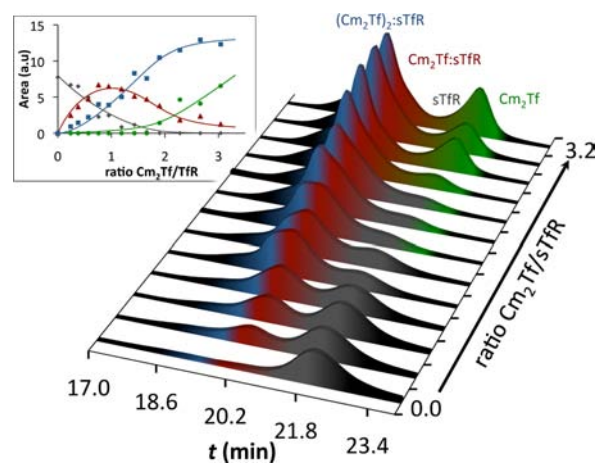


**Figure 5.** Titration of sTfR (0.95  $\mu\text{M}$ ) with  $\text{Cm}_2\text{Tf}$  (0 to 3.2 equiv) followed by HPLC (100 mM  $\text{NH}_4\text{HCO}_3$ , pH 7.4, 25 °C). Chromatograms were deconvoluted to follow the formation and/or disappearance of the 4 occurring species. The inset shows the extracted peak areas (data points) and corresponding fits (lines, two binding-site model) for  $(\text{Cm}_2\text{Tf})_2:\text{sTfR}$  (blue line, blue squares),  $(\text{Cm}_2\text{Tf})_2:\text{sTfR}$  (red line, red triangles), sTfR (gray line, gray diamonds) and  $\text{Cm}_2\text{Tf}$  (green line, green circles).

the chromatographic patterns resulting from solutions with  $\text{M}_2\text{Tf}:\text{sTfR}$  ratios varying from 0:1 to 3.2:1, and determine sequential sTfR equilibrium dissociation constants  $K_{d1}$  and  $K_{d2}$  (corresponding to the stepwise dissociation of  $(\text{M}_2\text{Tf})_2:\text{sTfR}$  and  $(\text{M}_2\text{Tf})_2:\text{sTfR}$ , respectively), for the different  $\text{M}_2\text{Tf}$  complexes. This assay was first benchmarked using the binding of  $\text{Fe}_2\text{Tf}$  to the sTfR and the obtained  $K_d$  values fall perfectly within the ranges reported in the literature using other techniques.<sup>16</sup> Analysis of the data afforded  $K_{d1}$  values slightly higher than that of the endogenous  $\text{Fe}_2\text{Tf}$  for both  $\text{Fe}_\text{C}\text{Cm}_\text{N}\text{Tf}$  and  $\text{Cm}_2\text{Tf}$ , while the binding of one unit of  $\text{Cm}_\text{C}\text{Fe}_\text{N}\text{Tf}$  appeared as tight as for  $\text{Fe}_2\text{Tf}$  (Table 1). In contrast, both mixed protein species,  $\text{Fe}_\text{C}\text{Cm}_\text{N}\text{Tf}$  and  $\text{Cm}_\text{C}\text{Fe}_\text{N}\text{Tf}$ , displayed  $K_{d2}$  values similar to  $\text{Fe}_2\text{Tf}$ , while the value determined for  $\text{Cm}_2\text{Tf}$  was 1 order of magnitude higher, indicating better recognition of the Fe-containing exogenous complexes by the sTfR receptor, in comparison to  $\text{Cm}_2\text{Tf}$ .

## DISCUSSION

The luminescence of  $\text{Cm}^{3+}$  emitted from the complex  $\text{Cm}_2\text{Tf}$  excited at 280 nm was estimated to be at least  $10^7$  times more intense than that observed with  $\text{Cm}_2\text{Tf}$  excited at 397 nm. Such high emission levels are attained as a result of efficient energy transfer from the Tf Cm-binding tyrosinate residues to the metal center. Curium is the only An(III) for which this process, commonly referred to as the antenna effect in lanthanide luminescence studies,<sup>22,23</sup> has been observed in coordination complexes,<sup>43–47</sup> albeit rarely. However, the complexation of Cm by Tf provides the first macromolecular example of ligand-enhanced Cm emission, and the high molar absorptivity of the protein results in a highly efficient antenna, notwithstanding the low quantum yields ( $\sim 1\%$ ) measured for the corresponding 1:1 and 1:2 complexes. Despite the similar electronic configurations of  $\text{Cm}^{3+}$  and  $\text{Gd}^{3+}$ , the emissive properties of  $\text{Cm}^{3+}$  are considered closer to those of  $\text{Eu}^{3+}$  and  $\text{Tb}^{3+}$ , due to the respective energy gaps of these metal ions. Prior laser-induced fluorescence studies with very large photon flux have used direct excitation ( $\lambda_{\text{exc}} = 395$  nm) of  $\text{Eu}^{3+}$  in  $\text{Eu}_2\text{Tf}$  to resolve the two Tf metal-binding sites.<sup>48</sup> However, no luminescence signal was observed after indirect protein excitation ( $\lambda_{\text{exc}} = 280$  nm) of the  $\text{Eu}_2\text{Tf}$  complex in the present study, revealing a lack of sensitization of the  $\text{Eu}^{3+}$  ions. This result contrasts with the strongly sensitized sharp luminescence of  $\text{Tb}^{3+}$  ions in the  $\text{Tb}_2\text{Tf}$  complex.<sup>38</sup> The emitting excited states of  $\text{Cm}^{3+}$  and  $\text{Eu}^{3+}$ ,  ${}^6\text{D}_{7/2}$  and  ${}^5\text{D}_0$ , respectively, are almost at the same energy level of  $\sim 17\,000\text{ cm}^{-1}$ ,<sup>49</sup> while the  $\text{Tb}^{3+}$  emitting state  ${}^5\text{D}_4$  is slightly higher in energy ( $\sim 18\,500\text{ cm}^{-1}$ ). Antenna sensitization usually occurs via the excited triplet state of the ligand and is optimized when the latter is at least  $1850\text{ cm}^{-1}$  higher in energy than the metal emitting states,<sup>50</sup> which should make Tf a good antenna chromophore for all three metals. However, in the case of  $\text{Eu}^{3+}$ , low lying ligand-to-metal charge-transfer states can be readily accessed when higher excitation energies (e.g.,  $\geq 30\,000\text{ cm}^{-1}$ ) are used,<sup>51</sup> which may explain why Tf sensitizes the luminescence of  $\text{Cm}^{3+}$  ( $\lambda_{\text{em}} = 619$  nm) and  $\text{Tb}^{3+}$  ( $\lambda_{\text{em}} = 545$  nm) but not  $\text{Eu}^{3+}$ . The antenna effect can therefore be used as a powerful discrimination tool to identify these trivalent f-elements, since indirect excitation of Tf will lead to sharp and intense, but distinct, emissions for  $\text{Tb}^{3+}$  and  $\text{Cm}^{3+}$  and no emission in the case of  $\text{Eu}^{3+}$ . While UV–visible spectroscopy provides some information on the coordination mode of the metals within the Tf binding site, such as the characteristic tyrosine-binding mode, time-resolved luminescence analysis allows for the direct determination of the number of inner sphere water molecules and thereby the coordination number of the metal ion. In this study, two inner sphere water molecules were found in both Cm-binding sites of  $\text{Cm}_2\text{Tf}$ . These results suggest a minimum coordination number of 8 for each metal ion in  $\text{Cm}_2\text{Tf}$ , with two  $\text{H}_2\text{O}$  ligands in addition to the protein ligands, similar to what has been proposed for  $\text{Tb}_2\text{Tf}$ .<sup>38</sup> Such numbers are common for trivalent f-elements, but are distinct from the coordination number of 6 previously reported for lactoferrin-bound cerium(IV) ( $r(\text{N}6) = 0.87\text{ \AA} - r(\text{N}8) = 0.97\text{ \AA}$ )<sup>52</sup> and Tf-bound Pu(IV) ( $r(\text{N}6) = 0.86\text{ \AA} - r(\text{N}8) = 0.96\text{ \AA}$ ),<sup>20</sup> based on X-ray diffraction and small-angle X-ray scattering data, respectively. The coordination of  $\text{UO}_2^{2+}$  by Tf has also been investigated previously, suggesting yet another binding mode that excludes the histidine from the equatorial plane of the metal ion.<sup>12</sup> These differences in Tf coordination illustrate the relative flexibility of the protein in

binding different metal ions, based on their intrinsic charge, radius and oxidation state. However, they also affect the stability and overall conformation of the corresponding complexes.

Following spectrophotometric methods previously reported with lanthanides,<sup>25</sup> four titration approaches were taken to measure the two sequential association constants of  $\text{Cm}^{3+}$  with Tf,  $\log K_{\text{C}}$  and  $\log K_{\text{N}}$ . Emission spectra (after direct and indirect excitation of  $\text{Cm}^{3+}$ ) and lifetimes were recorded simultaneously, providing additional species-specific data sets for data refinement. As expected,<sup>53</sup> the much larger ionic radii of  $\text{Cm}^{3+}$  in comparison to  $\text{Fe}^{3+}$  leads to weaker complexation, and both stability constants (8.8 and 7.0, respectively) are dramatically lower than the corresponding values for  $\text{Fe}^{3+}$  (21.9 and 20.6)<sup>54</sup> and  $\text{Pu}^{4+}$  (21.3),<sup>5,10</sup> lower than the  $\text{UO}_2^{2+}$  values (12.4 and 11.4),<sup>55–57</sup> but still in the typical range of values determined for lanthanides. Similar to what is reported for lanthanides,<sup>58–60</sup> the C-terminal site of Tf has a stronger binding affinity towards  $\text{Cm}^{3+}$  than the N-terminal site. Although this study provides the first experimental determination of Tf complex formation constants with Cm, several estimated values ranging over 4 orders of magnitude had previously been reported. Linear free energy relationships (LFER) correlating reference low molecular weight complex formation constants of  $\text{Nd}^{3+}$  and  $\text{Sm}^{3+}$  with data available for  $\text{Cm}^{3+}$  resulted in the calculated value  $\log K_{\text{C}} = 6.5 \pm 0.8$ .<sup>25</sup> While LFER is a benchmark method to accurately predict stability constants with low molecular weight ligands, significant variations (up to 2 log units) have been observed between the calculated and experimental Tf-binding constant values with lanthanides such as  $\text{Sm}^{3+}$ ,  $\text{Gd}^{3+}$  and  $\text{Tb}^{3+}$ ,<sup>60</sup> questioning the reliability of this model for macromolecular complexes. In a more recent report, higher values for  $\text{Cm}^{3+}$  complexation by Tf,  $\log K_{\text{C}} = 10.3$  and  $\log K_{\text{N}} = 8.7$ , were derived from correlations between the overall metal-binding constant of Tf and the first metal ion hydrolysis constant, with carbonate as a synergistic anion.<sup>5</sup> However, these correlations also provide Tf-binding constants significantly different from the corresponding experimental values for  $\text{Pu}^{4+}$  and  $\text{UO}_2^{2+}$ . These results emphasize the need for empirical determination of thermodynamic parameters of complexation, as the interpolation procedures for both methods may have taken into account the size and Lewis acidity of the different metal ions, but not necessarily steric effects inherent to the flexibility of the protein cavities or changes in the number of coordinated water molecules in the primary coordination layer of the metal ions.<sup>61</sup>

In healthy individuals, Tf is present at a serum concentration of 25–50  $\mu\text{M}$  but is only 30% saturated with Fe, with the following distribution: 27%  $\text{Fe}_2\text{Tf}$ , 23%  $\text{Fe}_\text{N}\text{Tf}$ , 11%  $\text{Fe}_\text{C}\text{Tf}$ , and 40% apo-Tf.<sup>24</sup> The different thermodynamic stabilities of the Tf complexes formed with Cm(III), Pu(IV), U(VI) could therefore account for the different distribution of the metals in blood (100%, 30% and 30% of  $\text{Pu}^{4+}$ ,  $\text{UO}_2^{2+}$ , and  $\text{Cm}^{3+}$  in blood, respectively, are reportedly bound by Tf);<sup>5</sup> however, the conformation of the corresponding protein-complexes is the major factor influencing their fate as Tf-bound species. The  $K_{\text{d}}$  values determined for the binding of  $\text{Cm}_2\text{Tf}$ ,  $\text{Fe}_\text{C}\text{Cm}_\text{N}\text{Tf}$ , and  $\text{Cm}_\text{C}\text{Fe}_\text{N}\text{Tf}$  to sTfR indicate that the tested Cm–Tf species appear to be recognized by the receptor with affinities relatively close to that of  $\text{Fe}_2\text{Tf}$  and higher than those previously found for  $\text{Pu-Tf}$ <sup>20</sup> and  $\text{UO}_2\text{-Tf}$  species.<sup>19</sup> TfR-mediated endocytosis is therefore a plausible pathway for entry of  $\text{Cm}^{3+}$  into a cell, consistent with the faster clearance of An(III) such as  $\text{Cm}^{3+}$

from the blood and higher liver uptake rate in comparison to other oxidation states.<sup>5,7</sup> It was also recently reported that only Pu<sub>C</sub>Fe<sub>N</sub>Tf can transport Pu through cellular membranes,<sup>20</sup> revealing a striking difference with what was observed with Cmand providing avenues to design highly discriminating systems between An(III) and An(IV) or Ln(III).

## CONCLUSIONS

This study demonstrates that luminescence spectroscopy combined with chromatography can provide detailed information on the coordination of Cm<sup>3+</sup> within biological systems through the use of specific intramolecular energy transfer processes, affording the first experimental report of thermodynamic parameters that drive the binding of Cm<sup>3+</sup> to proteins such as Tf and subsequent recognition by the cellular TfR receptor. The methods described here will therefore be applied further to investigate the mechanistic details of the biological transport of Cm<sup>3+</sup> and to determine the factors conveying the discrimination between Cm and other An and Ln ions.

## ASSOCIATED CONTENT

### Supporting Information

Determination of experimental procedures for spectroscopic titrations using Eu<sup>3+</sup> as a nonradioactive surrogate ion for Cm<sup>3+</sup>; determination of thermodynamic and photophysical parameters for the binding of Cm<sup>3+</sup> by human transferrin. This material is available free of charge via the Internet at <http://pubs.acs.org>.

## AUTHOR INFORMATION

### Corresponding Author

rjabergel@lbl.gov

### Notes

The authors declare no competing financial interest.

## ACKNOWLEDGMENTS

We thank Prof. Kenneth N. Raymond, Dr. David K. Shuh, Dr. Norman M. Edelstein, Dr. Guoxin Tian, and Dr. Petr Kuzmic for helpful discussions. Instrument acquisition and method development for the chromatography assays were supported by the National Institutes of Health (R.J.A., RAI087604Z); the experimental work on actinide-protein interactions was supported by the Director, Office of Science, of the U.S. Department of Energy under Contract No. DE-AC02-05CH11231, through a Laboratory Directed Research and Development program (R.J.A.), and by a U.S. Public Service Grant (A.B.M., R01 DK 21739).

## REFERENCES

- (1) National Council on Radiation Protection and Measurements. *Management of Persons Contaminated with Radionuclides Handbook: Recommendations of the National Council on Radiation Protection and Measurements*; National Council on Radiation Protection and Measurements: Bethesda, MD, 2009; Vol. 161.
- (2) Lumetta, G. J.; Thompson, M. C.; Penneman, R. A.; Eller, P. G. In *The Chemistry of the Actinide and Transactinide Elements*; Morss, L. R., Edelstein, N. M., Fuger, J., Eds.; Springer: Dordrecht, The Netherlands, 2011; pp 1397–1443.
- (3) Nash, K. L.; Madic, C.; Mathur, J. N.; Lacquement, J. In *The Chemistry of the Actinide and Transactinide Elements*; Morss, L. R., Edelstein, N. M., Fuger, J., Eds.; Springer: Dordrecht, The Netherlands, 2011; pp 2622–2798.

- (4) Durbin, P. W. In *The Chemistry of the Actinide and Transactinide Elements*; Morss, L. R., Edelstein, N. M., Fuger, J., Eds.; Springer: Dordrecht, The Netherlands, 2011; pp 3339–3440.
- (5) Ansoborlo, E.; Prat, O.; Moisy, P.; Den Auwer, C.; Guillaud, P.; Carriere, M.; Gouget, B.; Duffield, J.; Doizi, D.; Vercouter, T.; Moulin, C.; Moulin, V. *Biochimie* **2006**, *88*, 1605–1618.
- (6) Durbin, P. W. *Health Phys.* **2008**, *95*, 465–492.
- (7) Ménétrier, F.; Taylor, D. M.; Comte, A. *Appl. Radiat. Isot.* **2008**, *66*, 632–647.
- (8) Turner, G. A.; Taylor, D. M. *Phys. Med. Biol.* **1968**, *13*, 535–546.
- (9) Cooper, J. R.; Gowing, H. S. *Int. J. Radiat. Biol.* **1981**, *40*, 569–572.
- (10) Taylor, D. M. *J. Alloys Compd.* **1998**, *271–273*, 6–10.
- (11) Mason, A. B.; Byrne, S. L.; Everse, S. J.; Roberts, S. E.; Chasteen, N. D.; Smith, V. C.; MacGillivray, R. T. A.; Kandemir, B.; Bou-Abdallah, F. J. *Mol. Recognit.* **2009**, *22*, 521–529.
- (12) Wally, J.; Halbrooks, P. J.; Vonrhein, C.; Rould, M. A.; Everse, S. J.; Mason, A. B.; Buchanan, S. K. *J. Biol. Chem.* **2006**, *281*, 24934–24944.
- (13) Li, H.; Sun, H.; Qian, Z. M. *Trends Pharmacol. Sci.* **2002**, *23*, 206–209.
- (14) Adams, T. E.; Mason, A. B.; He, Q.-Y.; Halbrooks, P. J.; Briggs, S. K.; Smith, V. C.; MacGillivray, R. T. A.; Everse, S. J. *J. Biol. Chem.* **2003**, *278*, 6027–6033.
- (15) Cheng, Y.; Zak, O.; Aisen, P.; Harrison, S. C.; Walz, T. *Cell* **2004**, *116*, 565–576.
- (16) Byrne, S. L.; Leverence, R.; Klein, J. S.; Giannetti, A. M.; Smith, V. C.; MacGillivray, R. T. A.; Kaltashov, I. A.; Mason, A. B. *Biochem.* **2006**, *45*, 6663–6673.
- (17) Du, X.; Zhang, T.; Yuan, L.; Zhao, Y.; Li, R.; Wang, K.; Yan, S. C.; Zhang, L.; Sun, H.; Qian, Z. *Eur. J. Biochem.* **2002**, *269*, 6082–6090.
- (18) Vidaud, C.; Gourion-Arsiquaud, S.; Rollin-Genetet, F.; Torne-Celer, C.; Plantevin, S.; Pible, O.; Berthomieu, C.; Quéméneur, E. *Biochem.* **2007**, *46*, 2215–2226.
- (19) Hémadi, M.; Ha-Duong, N.-T.; Plantevin, S.; Vidaud, C.; El Hage Chahine, J.-M. *J. Biol. Inorg. Chem.* **2010**, *15*, 497–504.
- (20) Jensen, M. P.; Gorman-Lewis, D.; Aryal, B.; Paunesku, T.; Vogt, S.; Rickert, P. G.; Seifert, S.; Lai, B.; Woloschak, G. E.; Soderholm, L. *Nat. Chem. Biol.* **2011**, *7*, 560–565.
- (21) Edelstein, N. M.; Klenze, R.; Fanghanel, T.; Hubert, S. *Coord. Chem. Rev.* **2006**, *250*, 948–973.
- (22) D'Aléo, A.; Pointillart, F.; Ouahab, L.; Andraud, C.; Maury, O. *Coord. Chem. Rev.* **2012**, *256*, 1604–1620.
- (23) Bünzli, J.-C. G.; Pigué, C. *Chem. Soc. Rev.* **2005**, *34*, 1048.
- (24) Byrne, S.; Mason, A. *J. Biol. Inorg. Chem.* **2009**, *14*, 771–781.
- (25) Harris, W. R. *Inorg. Chem.* **1986**, *25*, 2041–2045.
- (26) Eckenroth, B. E.; Steere, A. N.; Chasteen, N. D.; Everse, S. J.; Mason, A. B. *Proc. Natl. Acad. Sci. U.S.A.* **2011**, *108*, 13089–13094.
- (27) Sturzbecher-Hoehne, M.; Ng Pak Leung, C.; D'Aléo, A.; Kullgren, B.; Prigent, A.-L.; Shuh, D. K.; Raymond, K. N.; Abergel, R. *J. Dalton Trans.* **2011**, *40*, 8340–8346.
- (28) Chen, R. F. *Anal. Lett.* **2011**, *1*, 35–42.
- (29) Lakowicz, J. R. *Principles of Fluorescence Spectroscopy*; Springer, New York, 2006.
- (30) Abergel, R. J.; D'Aleo, A.; Ng Pak Leung, C.; Shuh, D. K.; Raymond, K. N. *Inorg. Chem.* **2009**, *48*, 10868–10870.
- (31) Gans, P.; O'Sullivan, B. *Talanta* **2000**, *51*, 33–37.
- (32) Gans, P.; Sabatini, A.; Vacca, A. *Talanta* **1996**, *43*, 1739–1753.
- (33) Gans, P.; Sabatini, A.; Vacca, A. *Ann. Chim.* **1999**, *89*, 45–49.
- (34) Gans, P.; Sabatini, A.; Vacca, A. *HypSpec*; Leeds, U.K., Florence, Italy, 2008.
- (35) Kuzmic, P. *Anal. Biochem.* **1996**, *237*, 260–273.
- (36) Carnall, W. T. *J. Chem. Phys.* **1992**, *96*, 8713.
- (37) Sykora, R. E.; Assefa, Z.; Haire, R. G.; Albrecht-Schmitt, T. E. *Inorg. Chem.* **2005**, *44*, 5667–5676.
- (38) White, G. F.; Litvinenko, K. L.; Meech, S. R.; Andrews, D. L.; Thomson, A. J. *Photochem. Photobiol. Sci.* **2004**, *3*, 47–55.

- (39) Kimura, T.; Choppin, G. R. *J. Alloys Compd.* **1994**, *213-214*, 313–317.
- (40) Harris, W. R. In *Less Common Metals in Proteins and Nucleic Acid Probes*; Springer: Berlin Heidelberg, 1998; Vol. 92, pp 121–162.
- (41) Wang, Z.; Felmy, A. R.; Xia, Y.; Mason, M. J. *Radiochim. Acta* **2003**, *91*, 329–338.
- (42) Martell, A. E.; Smith, R. M.; Motekaitis, R. J. *NIST Standard Reference Database 46*; National Institute of Standards and Technology: Gaithersburg, MD, 2004.
- (43) Assefa, Z.; Yaita, T.; Haire, R. G.; Tachimori, S. *Inorg. Chem.* **2003**, *42*, 7375–7377.
- (44) Assefa, Z.; Yaita, T.; Haire, R. G.; Tachimori, S. *J. Solid State Chem.* **2005**, *178*, 505–510.
- (45) Panak, P.; Klenze, R.; Kim, J. I.; Wimmer, H. *J. Alloys Compd.* **1995**, *225*, 261–266.
- (46) Wang, X. K.; Rabung, T.; Geckeis, H.; Panak, P. J.; Klenze, R.; Fanghänel, T. *Radiochim. Acta* **2004**, *92*, 691–695.
- (47) Moll, H.; Bernhard, G. *J. Coord. Chem.* **2007**, *60*, 1795–1807.
- (48) O'Hara, P. B.; Bersohn, R. *Biochemistry* **1982**, *21*, 5269–5272.
- (49) Kimura, T.; Nagaishi, R.; Kato, Y.; Yoshida, Z. *Radiochim. Acta* **2001**, *89*, 125.
- (50) Latva, M.; Takalo, H.; Mikkala, V.-M.; Matachescu, C.; Rodríguez-Ubis, J. C.; Kankare, J. *J. Lumin.* **1997**, *75*, 149–169.
- (51) Kusaba, M.; Nakashima, N.; Kawamura, W.; Izawa, Y.; Yamanaka, C. *Chem. Phys. Lett.* **1992**, *197*, 136–140.
- (52) Baker, H. M.; Baker, C. J.; Smith, C. A.; Baker, E. N. *J. Biol. Inorg. Chem.* **2000**, *5*, 692–698.
- (53) Chipperfield, A. R.; Taylor, D. M. *Nature* **1968**, *219*, 609–610.
- (54) Sun, H.; Li, H.; Sadler, P. J. *Chem. Rev.* **1999**, *99*, 2817–2842.
- (55) Michon, J.; Frelon, S.; Garnier, C.; Coppin, F. *J. Fluoresc* **2010**, *20*, 581–590.
- (56) Scapolan, S.; Ansorborlo, E.; Moulin, C.; Madic, C. *Radiat. Prot. Dosim.* **1998**, *79*, 505–508.
- (57) Montavon, G.; Apostolidis, C.; Bruchertseifer, F.; Repinc, U.; Morgenstern, A. *J. Inorg. Biochem.* **2009**, *103*, 1609–1616.
- (58) Yang, B. S.; Harris, W. R. *Acta Chim. Sin.* **1999**, *57*, 503–509.
- (59) Harris, W. R.; Chen, Y. *Inorg. Chem.* **1992**, *31*, 5001–5006.
- (60) Abdollahi, S.; Harris, W. R. *Iran. J. Chem. Chem. Eng.* **2006**, *25*, 45–52.
- (61) Rizkalla, E. N.; Choppin, G. R. *J. Alloys Compd.* **1992**, *180*, 325–336.